



Modeling intrinsic vulnerability of complex karst aquifers: modifying the COP method to account for sinkhole density and fault location

Natalie A. Jones¹ · Jered Hansen² · Abraham E. Springer¹ · Cynthia Valle³ · Benjamin W. Tobin^{2,4}

Received: 12 April 2019 / Accepted: 27 September 2019 / Published online: 11 November 2019
© Springer-Verlag GmbH Germany, part of Springer Nature 2019

Abstract

This study investigates a method of karst-aquifer vulnerability modeling that modifies the concentration-overburden-precipitation (COP) method to better account for structural recharge pathways through noncarbonate rocks, and applies advancements in remote-sensing sinkhole identification. Karst aquifers are important resources for human and agricultural needs worldwide, yet they are often highly complex and have high vulnerability to contamination. While many methods of estimating intrinsic vulnerability of karst aquifers have been developed, few methods acknowledge the complication of layered karst aquifer systems, which may include interactions between carbonate and noncarbonate rocks. This paper describes a modified version of the COP method applied to the Kaibab Plateau, Arizona, USA, the primary catchment area supplying springs along the north side of the Grand Canyon. The method involves two models that, together, produce higher resolution and greater differentiation of vulnerability for both the deep and perched aquifers beneath the Kaibab Plateau by replacing the original sinkhole distance parameter with sinkhole density. Analyses indicate that many karst regions would benefit from the methodology developed for this study. Regions with high-resolution elevation data would benefit from the incorporation of sinkhole density data in aquifer vulnerability assessments, and deeper semi-confined karst aquifers would benefit greatly from the consideration of fault location.

Keywords Karst · Vulnerability mapping · Groundwater vulnerability · Semi-arid region · USA

Introduction

Karst aquifers are significant resources for human and agricultural uses across the world. Despite only covering 12% of the earth's surface, karst aquifers contain some of the largest and most productive springs, and directly supply up to 25% of the world population with water for drinking, agriculture, and other water needs (Ford and Williams 2007), while also providing extended seasonal storage for base flow of rivers and subsequent water use downstream (Tobin 2013).

Karst aquifers are highly vulnerable to contamination because rapid infiltration in sinkholes (the word sinkhole will be used throughout this paper as a synonym for dolines, swallow holes, cenotes, etc.) and swallets allows focused flow through the epikarst and vadose zone that results in reduced travel time (Zwahlen 2004; Goldscheider and Drew 2007). This increased vulnerability due to karst features has inspired the development of vulnerability models used to better map and quantify the intrinsic vulnerability of karst terrain (Daly et al. 2002; Doerfliger et al. 1999; Goldscheider et al. 2000; Kavouri et al. 2011; Ravbar and Goldscheider 2007; Vias et al. 2006). Intrinsic vulnerability is a term that describes the vulnerability of groundwater to contaminants where the properties and location of the individual contaminant are not considered (Daly et al. 2002).

The concentration-overburden-precipitation (COP) method is regarded as a detailed, easy-to-use, accurate method for modeling karst vulnerability in humid regions (Guastaldi et al. 2014; Iván and Mádl-Szonyi 2017; Marín et al. 2012; Polemio et al. 2009); however, it is limited by the assumption that surface karst features such as sinkholes, have a direct path to the underlying aquifer. The COP method assigns

✉ Natalie A. Jones
nataliejones.a@gmail.com

¹ School of Earth and Sustainability, Northern Arizona University, Flagstaff, AZ, USA

² Grand Canyon National Park, Flagstaff, AZ, USA

³ Nez Perce-Clearwater National Forests, Kamiah, ID, USA

⁴ Kentucky Geological Survey, University of Kentucky, Lexington, KY, USA

vulnerability categories based on a numerical range of 0–15, with zero being the highest possible vulnerability, and 15 being the lowest possible vulnerability. The COP method assigns any region within 500 m of a sinkhole a value of zero, resulting in a categorization of “very high vulnerability” for that region, regardless of other factors (Vías et al. 2006). All other regions are assumed to be controlled by diffuse recharge.

The COP method does not consider the presence of structural features or the variations of recharge capacity of individual sinkholes that may affect aquifer vulnerability. These factors are potentially critical in evaluating the vulnerability of aquifers located in dry environments that often have negligible diffuse recharge and naturally thick overburden (Scanlon et al. 2002, 2006; Marín et al. 2012; Vías et al. 2006). In semi-arid and arid environments, aquifers are often deep below the surface and recharge is primarily focused along ephemeral stream channels, topographic depressions, and zones of faulted and fractured rock (Healy 2010; Scanlon et al. 2002, 2006). Therefore, if surface karst exists, direct connections from surface karst to aquifers cannot be assumed, especially when noncarbonate strata are present.

In karst aquifer systems, sinkholes help to focus aquifer recharge and increase aquifer vulnerability. However, even in humid environments karst surface features may not have direct connection to aquifers below, and more complex groundwater mixing may occur, slowing transit time into and through the aquifer (Bear 2007; Ford and Williams 2007). For example, when perched aquifers are present on top of aquitards, horizontal flow will occur along the aquitard boundary until a break in the aquitard allows leakage and recharge into underlying layers. Additionally, underlying conduits beneath sinkholes can vary greatly, resulting in rapid water transport through sinkholes connected to large conduits and slower transport through sinkholes connected to fracture systems that can be easily clogged with silt and clay (Panno et al. 2013). While connectivity of a sinkhole to a water source is best determined through quantitative dye tracing, simple geospatial patterns such as sinkhole density and distribution, can also be used to estimate vulnerability variations in sinkhole plains on a local-to-regional scale (Panno et al. 2008; Lindsey et al. 2010).

Other researchers have highlighted the importance of sinkhole density to groundwater vulnerability, but have not implemented COP method modifications to account for this (Moreno-Gomez et al. 2018). A study comparing sinkhole densities and groundwater contaminants between several regions in the eastern United States showed that high sinkhole density correlates with an increase in groundwater contaminants (Lindsey et al. 2010). High sinkhole densities also correlate with the presence of conduits and concentrated flow paths: regions of high-volume conduit flow tend to have larger conduits and higher rates of dissolution which in turn leads to increased sinkhole

formation. Therefore regions of high sinkhole density are more likely to have greater conduit capacity and groundwater recharge contribution than regions of low sinkhole density (Panno et al. 2008). Furthermore, a comparison of fault and fracture location and sinkhole density on the semi-arid Kaibab Plateau, AZ, USA, showed a correlation between zones of high sinkhole density and the location of faults (Jones et al. 2017), strengthening the assumption that faults present in zones of high sinkhole density are hydrologically active and are potentially delivering water from surface karst features to underlying aquifers.

This study addresses shortcomings in the application of the COP method in arid and semiarid environments to assess the overall vulnerability of karst aquifers. The purpose of this study is to compare the original COP methodology with a modified method that uses sinkhole density as well as the location of faulted and fractured rock to model intrinsic vulnerability in deep, multilayered aquifer systems that have abundant surface karst. The resulting two models created greater spatial variation in vulnerability class predictions across our study area that better reflect recharge patterns of a region containing a stacked perched and deep aquifer system. These proposed modifications can be applied to a variety of aquifer systems and climates and can improve estimates of intrinsic vulnerability to contamination of karst aquifers, especially in regions that have limited karst, geophysical, and tracer survey data.

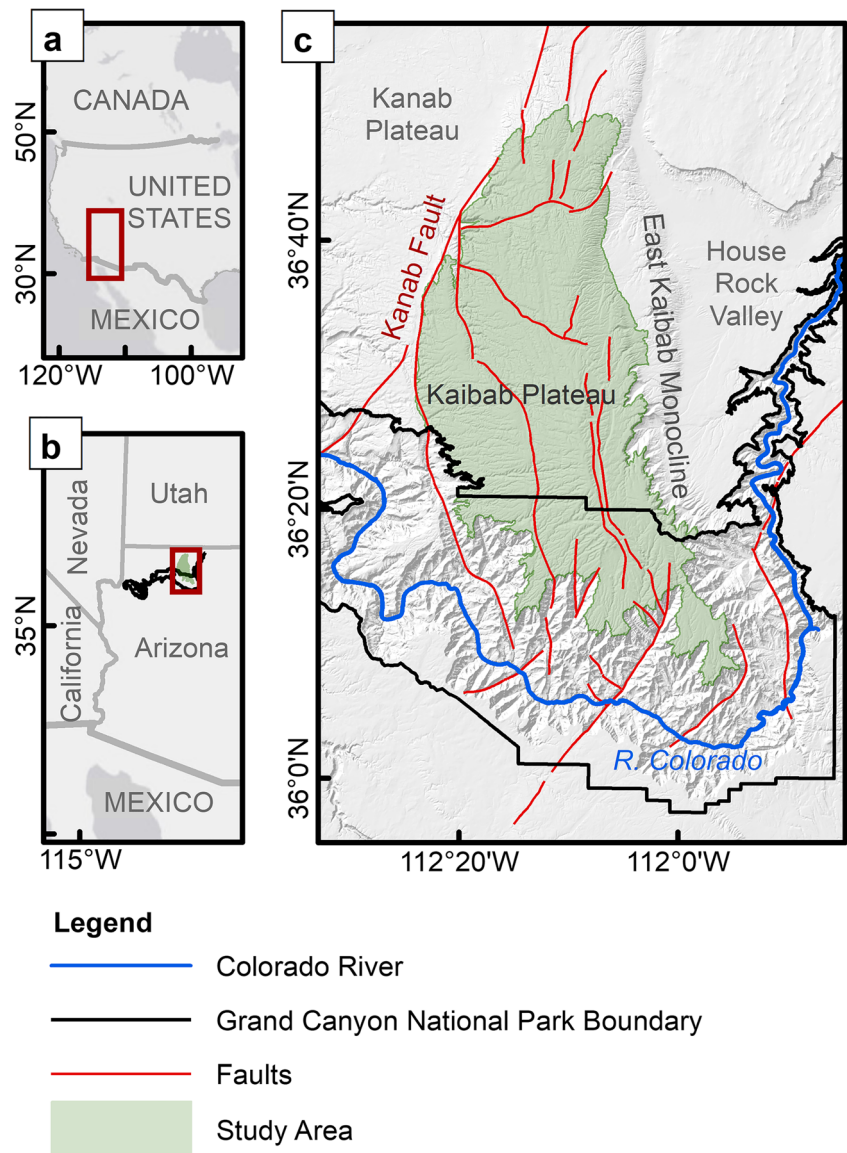
Materials and methods

Study area

The Kaibab Plateau is located in northern Arizona, USA, and is part of the Colorado Plateau physiographic province reaching a maximum elevation of 2,807 m (Figs. 1 and 2). It is bounded by the East Kaibab monocline to the east and the Kanab fault zone to the west (Fig. 1; Huntoon 1970). The southern boundary is marked abruptly by the sheer walls of the Grand Canyon with the Colorado River flowing at elevations below 850 m (Huntoon 1970, 1974). All of the surface geology within the study area is carbonate.

The landscape is covered predominantly by upper montane mixed-conifer and ponderosa pine forests, with meadows of short grassland occupying some basin and valley floors (Huntoon 1974; O'Donnell et al. 2018). The abundant, steep valleys on the plateau contain few active surface streams, generally poorly defined or nonexistent due to high evapotranspiration demands and/or focused groundwater percolation. While the area receives on average 62.7 cm of precipitation comprised of rain and snow (NOAA NCEI 2013), collection of surface runoff in sinkholes is limited to occasional severe

Fig. 1 Kaibab Plateau study area and geologic faults in the Colorado Plateau physiographic province north of the Grand Canyon, Arizona, USA: **a** The United States, Canada, and Mexico, with the red rectangle representing the frame extent of part **b**; **b** shows Arizona and the neighboring states and country, including the outline of Grand Canyon National Park and the frame extent of part **c**; **c** shows a shaded relief image of the study area and surrounding region. The faults displayed are approximate locations of major faults in the area



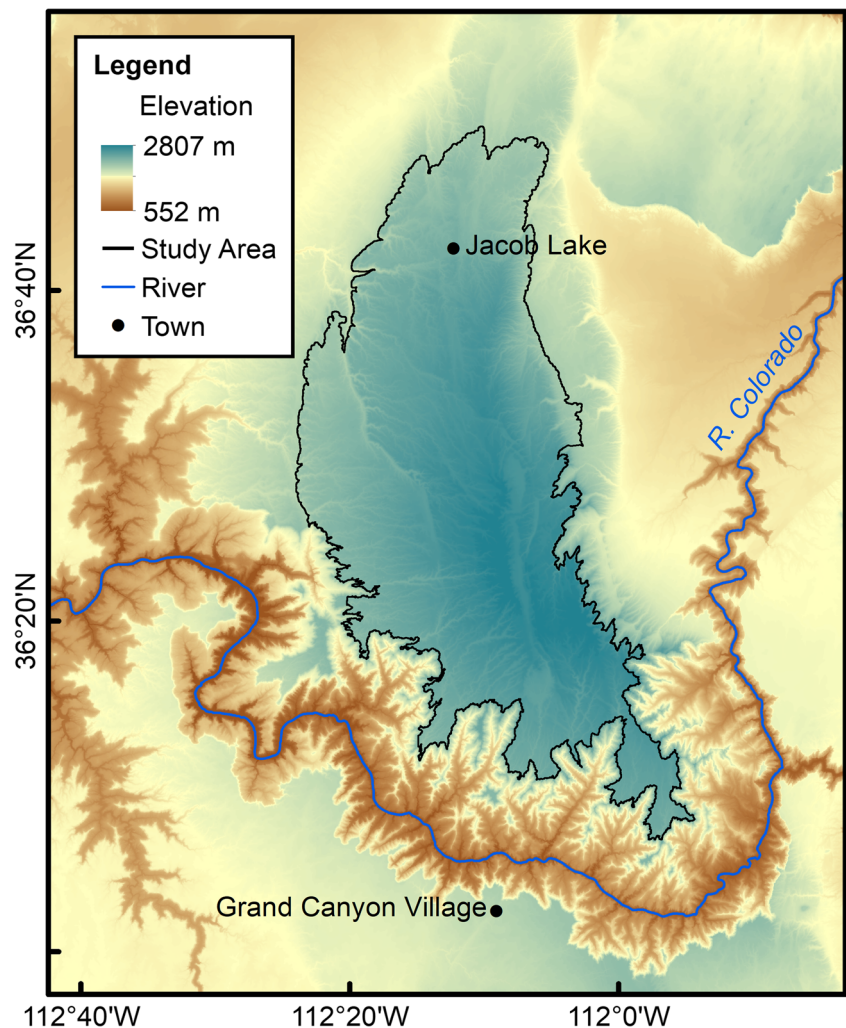
monsoon storm events during the summer months and snow-melt in the spring (Huntoon 1974).

Beneath the Kaibab Plateau surface are two karst aquifers, the Coconino aquifer which is perched above the Redwall-Muav aquifer (R aquifer, Fig. 3; Crossey et al. 2006; Huntoon 2000). The Coconino aquifer in this region has an average thickness of 300 m and is composed of the Kaibab Formation, the Toroweap Formation, and the Coconino Sandstone (McKee 1969). The Kaibab and Toroweap formations are both highly soluble, resulting in the epigenic formation of dissolved conduits and closed depressions throughout the region (Huntoon 1970, 1974). Between the Coconino and the R aquifers are siliciclastic confining units of the Hermit Shale and the Supai Group (Huntoon 1974, 1981, 2000). Both the Hermit Shale and Supai Group, while confining to some vertical water flow, are highly fractured near structural features, allowing for substantial recharge from the shallow Coconino aquifer to the underlying R

aquifer along parallel and subparallel fractures related to the faults (Huntoon 1974; Jones et al. 2017).

The R aquifer is composed primarily of the carbonates of the Redwall, Temple Butte, and Muav Formations (McKee and Gutschick 1969; McKee and Resser 1945). Below the Muav Formation is the Bright Angel Shale, the surface of which forms a regional aquitard. All of the R aquifer units are predominantly composed of limestones and dolomites with relatively low primary porosity and substantial secondary and tertiary permeability due to dissolution. Much of the cave development is hypogenic in origin and currently isolated from the groundwater flow system; however, there is still a substantial amount of karst development occurring as a result of modern karst processes (Hill and Polyak 2010). Current groundwater flow paths are responsible for a series of large caves formed due to these epigenic processes and result in R aquifer springs that are generally larger than Coconino aquifer

Fig. 2 Elevation model of Kaibab Plateau and surrounding region. Note the study area is outlined in black



springs, discharging on average and order of magnitude greater than Coconino aquifer springs. R aquifer spring responses are commonly flashy and variable depending on the season, precipitation intensity, and storm location (Huntoon 2000). Karstification throughout the Redwall and Muav formations occurs along fractures parallel and subparallel to regional faults and fractures (Hill and Polyak 2010).

Sinkholes provide the primary means of recharge to these two aquifers through a structurally controlled underlying conduit system (Huntoon 1974, 2000). While geophysical evidence of fault extent and conduit structure is limited, dye trace results suggest highly variable flow times from sinkholes to springs, suggesting other features may be driving flow dynamics (Jones et al. 2017). Sinkhole distribution and morphology above conduits can be indicative of conduit size and ability to recharge underlying aquifers and may play a role in this flow variability (Panno et al. 2008, 2013). Sinkhole densities on the Kaibab Plateau also correlate with locations of mapped faults and fractures, further indicating a structurally controlled conduit system (Panno et al. 2008; Jones et al. 2017).

Depression delineation

This study builds upon previous sinkhole mapping completed by Jones et al. (2017) by implementing Random Forests to improve automated differentiations between sinkholes and nonsinkhole depressions identified on the Kaibab Plateau (Breiman 2001). This method has been used in other karst regions in the past with high rates of successful sinkhole delineation (Miao et al. 2013; Zhu and Pierskalla 2016). In this study, sinkholes are defined as closed depressions resulting from a collapse of bedrock or soil or subsidence of soil from underlying conduit enlargement and/or piping of soil (Ford and Williams 2007). All sinkholes delineated in this study are assumed to have the ability to drain into the underlying conduit system.

Sinkholes were delineated from a 1 m² LiDAR-derived bare earth digital elevation model (DEM; Watershed Sciences 2012). The DEM was used to delineate depression features with automated GIS techniques in ArcGIS 10.5 (ESRI 2016; Watershed Sciences 2012) described in Jones et al. (2017). The resulting depression polygons were then

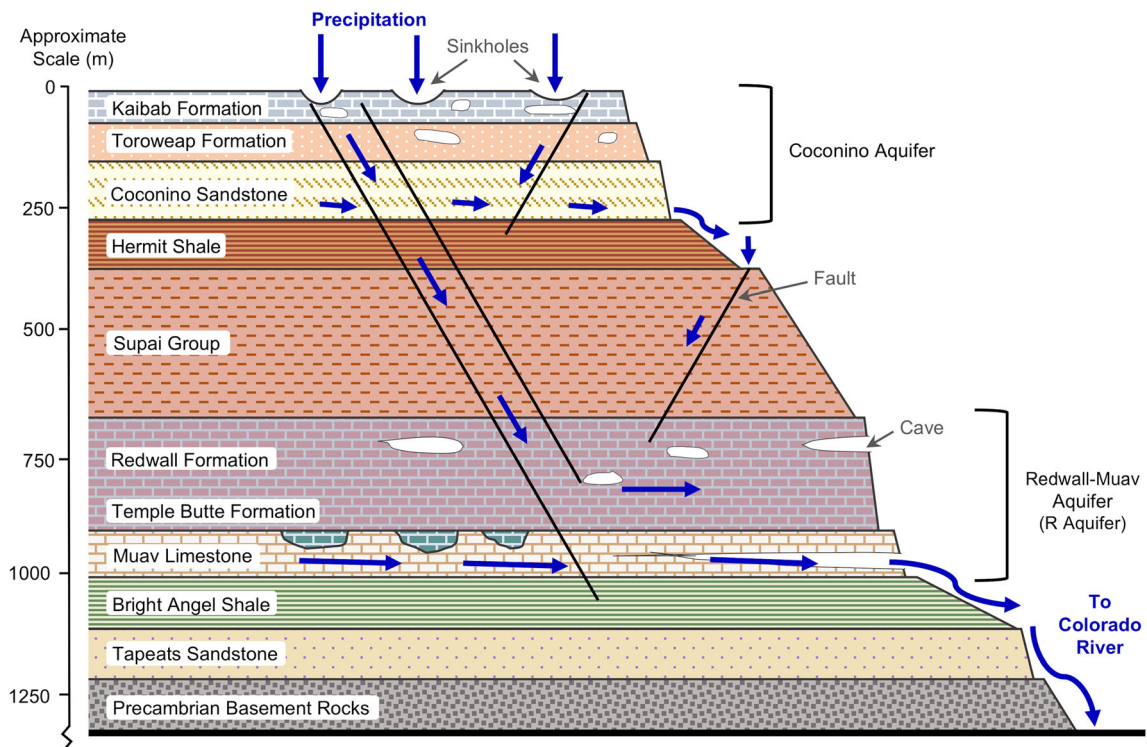


Fig. 3 Schematic diagram of the Kaibab Plateau hydrogeological system. Note the relative depths of the Coconino and R aquifers. Blue arrows represent the hypothetical flow of water through the geologic strata. Precipitation enters through sinkholes on the Kaibab Plateau, entering

the Coconino aquifer, and percolating to the R aquifer along permeable fault zones. Water discharges from springs in the Coconino and R aquifer and flows to the Colorado River

smoothed to round the blocky raster derived edge effects. The DEM used was not hydrologically corrected because accurate and comprehensive locations of culverts and stock tanks are not available; however, the depression classification process is believed to account for this error, resulting in a negligible impact to the final sinkhole delineation results.

Depression classification

A training dataset of depressions within 20 randomly generated 1-km² survey areas was generated by three people to manually identify true sinkhole depressions versus nonsinkhole depressions. The 3,057 training dataset depressions were visually inspected primarily against a LiDAR-derived hillshade dataset and secondarily an aerial photography to record whether each feature represented a “true” sinkhole, or a “false” sinkhole depression. In general, sinkhole geometry is much deeper and more circular than nonsinkhole depression geometry. This difference is often distinguishable in close visual observations of DEMs.

The resulting training dataset containing evaluation results (dependent variable) and 13 depression characteristics (independent variables) was used in an iterative modeling technique using the Random Forests regression method (Breiman 2001) and implemented in Salford Predictive

Modeler (Salford Systems 2016). Random Forests identified correlations between the dependent and independent results in the training dataset and ranked the dependent variables based on their ability to accurately classify the depressions (Table 1). Due to the lopsided number of depressions identified as false sinkholes (2,528 vs. 58), all depressions evaluated as “true” sinkholes by at least two of the three reviewers were assigned a weight of two. All other depressions were assigned a weight of one. The resulting model developed from the training dataset was then used by Random Forests in a “scoring” process to classify all Kaibab Plateau depressions based on their percent likelihood of being a true or false sinkhole. All depressions with a 50% or greater likelihood of being a true sinkhole were included in the final sinkhole dataset. A field survey of 64 sinkhole depressions was used to validate the percent accuracy of the Random Forests sinkhole results assess the frequency of false positives and false negatives. Depressions within a 4,000-m-radius sample area (limited for accessibility) were grouped by surface area size, and then randomly selected within each size class resulting in the following size distribution: 29 depressions smaller than 400 m², 20 depressions between 400 and 2,000 m², 10 depressions between 2,000 and 4,000 m², and 5 depressions greater than 4,000 m² in depression area. Sinkhole populations do not typically have standard bell-curve size distributions and have an exponential decrease

Table 1 Geometric variables used by Random Forests (Breiman 2001) to determine true sinkholes from false sinkhole depressions

Variable	Definition	Normalized percent contribution
Depth index D_i	$D_i = D_{\max} / \left(\frac{\sqrt{A}}{\pi} \right)$ where D_{\max} is the vertical distance (m) from pour point to lowest point within depression, and A (m^2) is the area of the depression in meters (Miao et al. 2013)	24.71
Mean depth D_{mean} (m)	Average depth (m) of a depression	20.42
Max depth D_{max} (m)	Vertical distance (m) from pour point to lowest point within the depression	19.81
Volume V (m^3)	Total volume (m^3) contained within depression	10.00
Depression concavity C_{mean}	Average rate of curvature around the perimeter of the depression, calculated using the curvature tool in ArcGIS (Zevenbergen and Thorne 1987)	7.43
Minimum bounding geometry width w (m)	Semi-minor axis length (m)	7.23
Area A (m^2)	Two-dimensional surface area covered by depression shape (m^2)	2.96
Minimum bounding geometry length l (m)	Semi-major axis length (m)	2.94
Circularity Circ	$\text{Circ} = 4\pi A / P^2$ where A is the area (m^2) of the depression, and P is the perimeter (m) of the depression (Davis 2002)	1.55
Perimeter P (m)	Length (m) of continuous line forming the boundary of the depression	1.15
Elongation Elong	$\text{Elong} = l/w$ where l is the semi-major axis length (m), and w is the semi-minor axis length (m)	1.14
Compactness Com	$\text{Com} = A/A_c$ where A is the area (m^2) of the depression, and A_c is the area (m^2) of the smallest perfect circle to encompass the depression (Li et al. 2013)	0.66
Orientation or (decimal degrees)	Orientation (decimal degrees) of semi-major axis of sinkhole calculated by the minimum bounding geometry tool of ArcGIS 10.5 (ESRI 2016)	0.0

Note that the 13 variables are ranked in order of effective importance (normalized percent contribution)

in sinkhole frequency as size increases (White 1988). These sample size classifications were selected to account for this expected size distribution.

COP method application

The COP method models aquifer vulnerability using a semi-quantitative approach. The method follows the European approach to vulnerability mapping in karst aquifers developed in the framework of COST Action (Daly et al. 2002; Iván and Mádl-Szonyi 2017; Vias et al. 2006). The model contains three basic components: the concentration of flow factor (C factor), the overlying layers factor (O factor), and the precipitation factor (P factor; Vias et al. 2006).

The C factor accounts for location of sinking streams and swallow holes (sinkholes), which are assumed to concentrate surface water into groundwater recharge points. The C factor also incorporates vegetation cover and slope into its calculations, which influence overland flow amounts and patterns. The final C factor for karst regions is calculated using the following equation:

$$C \text{ score} = dh \cdot ds \cdot sv \quad (1)$$

where dh is the distance from the recharge area to the swallow hole (sinkhole) value (between 0 and 1), ds is

the distance to sinking stream value (between 0 and 1), and sv is the slope-vegetation value (between 0.75 and 1) determined by amount of vegetation cover and degree of slope (Kass Green and Associates 2009; USDA Forest Service 2009; Watershed Sciences 2012).

The O factor estimates the protectiveness of layers of rock and soil overlying a given aquifer. In general, thicker and less permeable lithic layers are considered more protective than thin, highly permeable and/or karst-forming layers. Soil content and thickness is also considered, with clay-rich thick soil being most protective. The equation for calculating the O factor is:

$$O \text{ score} = [O_s] + [O_L] \quad (2)$$

where O_s is the soil subfactor value (between 0 and 5) corresponding to attenuation of infiltration due to the thickness, concentration, and distribution of soil cover, and O_L is the lithology subfactor, which is sum of values assigned to each rock layer overlying the aquifer describing the protectiveness of the unsaturated rock units above the aquifer based on rock type, thickness, existence secondary permeability (such as fracturing), and whether the units are confined or unconfined (Billingsley and Hampton 2000; Billingsley et al. 2008, 2012; Huntoon 2000).

The P factor accounts for precipitation quantity and temporal distribution with the equation:

$$P \text{ score} = P_Q + P_1 \quad (3)$$

where P_Q is the precipitation quantity value, a value between 0.2 and 0.4 describing the quantity of rainfall per year and P_1 is the temporal distribution value, which is a value between 0.2 and 0.6 representing the temporal distribution, which is determined by the mm of precipitation per year divided by the number of days with precipitation per year.

Once all C , O , and P scores are calculated, the COP method calls for the three scores to be multiplied together to create a final COP index. This COP index is categorized into a final COP map with vulnerability classes. A COP index score between 0 and 0.5 has very high vulnerability, a score between 0.5 and 1 has high vulnerability, a score between 1 and 2 has moderate vulnerability, a score between 2 and 4 has low vulnerability, and a score between 4 and 15 has very low vulnerability.

Shallow aquifer modifications

The O score and P scores for the shallow, Coconino aquifer were calculated according to the original COP method described in Vías et al. 2006. The values of these scores for the Kaibab Plateau fall within the range designated by the original methods. The C score was changed to better account for variability in vulnerability within a region containing sinkholes by replacing the distance from the recharge area to the swallow hole (dh) parameter with a sinkhole density (sd) parameter. The new parameter was chosen because sinkhole density correlates with aquifer contamination (Lindsey et al. 2010), and also with the presence of underlying conduits (Panno et al. 2008).

Sinkhole density was obtained using the Kernel Density function of ArcMAP 10.5, which calculates density from each sinkhole's geometric center point. This density was then reclassified (Table 2), where categories of vulnerability increase in equal intervals of 0.5 sinkholes per km². This categorization was chosen to match the original method of classification as closely as possible; in the original method, distances from sinkholes were categorized in equal intervals of 500 m, with 500 m from a sinkhole being the highest vulnerability level and a reclassification number of zero. If compared to sinkhole density, a region with four sinkholes per km² or greater would never be more than 500 m from a sinkhole, assuming all sinkholes were evenly spaced. Therefore, intervals of 0.5 sinkholes per km² were chosen so that the highest category of concentration vulnerability is assigned to any region with a sinkhole density greater than or equal to 4.5 sinkholes per km². Additionally, the new minimum classification value is 0.1 rather than 0.0, to allow for greater variability of

Table 2 Classification chart of sinkhole density per km² classes and the corresponding unitless sinkhole density parameter (sd) values

Sinkhole density	
Density per km ²	sd value
< 0.5	1.0
0.5–1	0.9
1–1.5	0.8
1.5–2	0.7
2–2.5	0.6
2.5–3	0.5
3–3.5	0.4
3.5–4	0.3
4–4.5	0.2
> 4.5	0.1

This classification is a key component of both the shallow and deep aquifer modified COP models

vulnerability once slope and vegetation parameters were applied.

Once the sinkhole density reclassifications were applied, sd was combined with the other C factor parameters using the following equation:

$$C \text{ score}_{\text{Coconino aquifer}} = sd \cdot sv \quad (4)$$

where sd is the sinkhole density value and sv is the slope-vegetation value. The distance from the recharge area to the swallow hole (ds) value was not included due to the absence of perennial surface streams.

The resulting C score, O score, and P score were multiplied together to create the final density-modified COP index for the perched Coconino aquifer. The index values were reclassified using the original COP classifications to create the final vulnerability model (Vías et al. 2006).

Deep aquifer modifications

The C score was modified to include the distance from recharge area to the faults (df) and sinkhole density (sd) parameters replacing the distance from recharge area to the swallow hole (ds) parameter. This combination was chosen for the deeper aquifer because of the role faults play in recharging deep aquifers along fault-driven ephemeral streams (Healy 2010; Scanlon et al. 2002, 2006), the connection between faults and sinkhole location previously observed on the Kaibab Plateau (Jones et al. 2017), and the correlation between high sinkhole density and the presence of productive aquifer flow paths (Lindsey et al. 2010; Panno et al. 2008). It is important to note that some faults are hydrologically sealed; however, jointing around the faults creates zones of high permeability parallel and subparallel to faults (Huntoon 1974). Therefore, in this study, fault locations are used as an

approximate location for these high-permeability fault zones. It is also assumed that all faults included in this model have zones of permeability that penetrate the entire sedimentary sequence from the surface to the R aquifer.

The distance from recharge areas to faults was calculated using a Euclidean Distance function applied to mapped faults in ArcMAP 10.5 (ESRI 2016; Ludington et al. 2005; Wilson et al. 1983). The distances were reclassified in 500-m increments (Table 3) similar to the *ds* parameter, but without including any values of zero (the new minimum value is 0.1) to allow for greater classification variability. The resulting *df* parameter was then averaged with the *sd* parameter to create the final deep aquifer flow concentration (*fc*) parameter.

$$fc = \frac{(df + sd)}{2} \quad (5)$$

Averaging the *df* and *sd* parameters assumes that the contribution of recharge to the R aquifer along faults and through sinkholes is equal. The final *C* score multiplied the *fc* parameters with the slope-vegetation (*sv*) parameter using the following equation:

$$C \text{ score}_{R \text{ Aquifer}} = fc \cdot sv \quad (6)$$

The *C*, *O*, and *P* scores were then multiplied together to create the final deep aquifer modified COP index. The index values were reclassified using the original COP classifications to create the final vulnerability model (Vías et al. 2006).

Results

Depression classification

Out of 257,519 total depressions, 6,973 were identified as true sinkholes by Random Forests (Fig. 4). Field validation

Table 3 Classification chart of the distance from the recharge area to the faults (m) and the corresponding unitless distance from the recharge area to faults parameter (*df*) values

Distance from the recharge area to faults	
Distance (m)	<i>df</i> value
<500	0.1
500–1,000	0.2
1,000–1,500	0.3
1,500–2,000	0.4
2,000–2,500	0.5
2,500–3,000	0.6
3,000–3,500	0.7
3,500–4,000	0.8
4,000–4,500	0.9
>4,500	1.0

This classification is a key component of the deep aquifer modified COP model

determined that 87.5% of all delineated depressions, 78.3% of sinkhole depressions, and 92.3% of nonsinkhole depressions were correctly classified.

Vulnerability

The results of the modified Coconino (shallow) and R (deep) aquifer vulnerability models were compared with the original, unmodified Coconino and R aquifer vulnerability COP models (Figs. 5 and 6). The modified models reduced the high vulnerability areas in the shallow Coconino aquifer from 97.2 to 39.4%, and from 94.0 to 0.1% in the deep, R aquifer (Table 4). All other vulnerability classes increased in percent cover. The modified shallow aquifer model indicates that the southern central portion of the Kaibab Plateau is highly vulnerable to contamination, while regions to the north and on the perimeter of the Kaibab Plateau are less vulnerable to contamination (Fig. 5). The modified deep aquifer model has higher vulnerability close to the location of faults (Fig. 6).

Discussion

The modified COP methods using sinkhole density instead of sinkhole distance produce vulnerability models based on landscape-scale karst geomorphology affecting recharge to deep aquifers in arid and semiarid environments rather than treating individual sinkholes equally. The original model produced little distinction between shallow, perched aquifer and deep, semiconfined aquifer vulnerability to contamination (Figs. 5a and 6a), while the modified models produced distinct differences between the shallow and deep aquifers (Figs. 5b and 6b). This contrast in vulnerability between the shallow and deep aquifers highlights the model effect of overburden—there is a great difference (over 600 m) in overlying rock thicknesses that act as an aquitard between these two aquifers (Huntoon 1974, 2000)—a characteristic that is poorly reflected in the original COP method models due to the value placed on distance from sinkholes.

A qualitative sensitivity analysis between the COP components reveals that the recharge concentration (*C* factor) is the main component controlling the variability in vulnerability on the Kaibab Plateau. While the original model has its strengths in identifying the significant role sinkholes play in contamination of karst aquifers, it disregards the differences in sinkhole hydrology that can be detected through sinkhole density (Panno et al. 2008). As a result, the original model likely overestimates vulnerability to contamination on the Kaibab Plateau because it assumes the infiltration capacity of all sinkholes is equal. Therefore, the original model does not

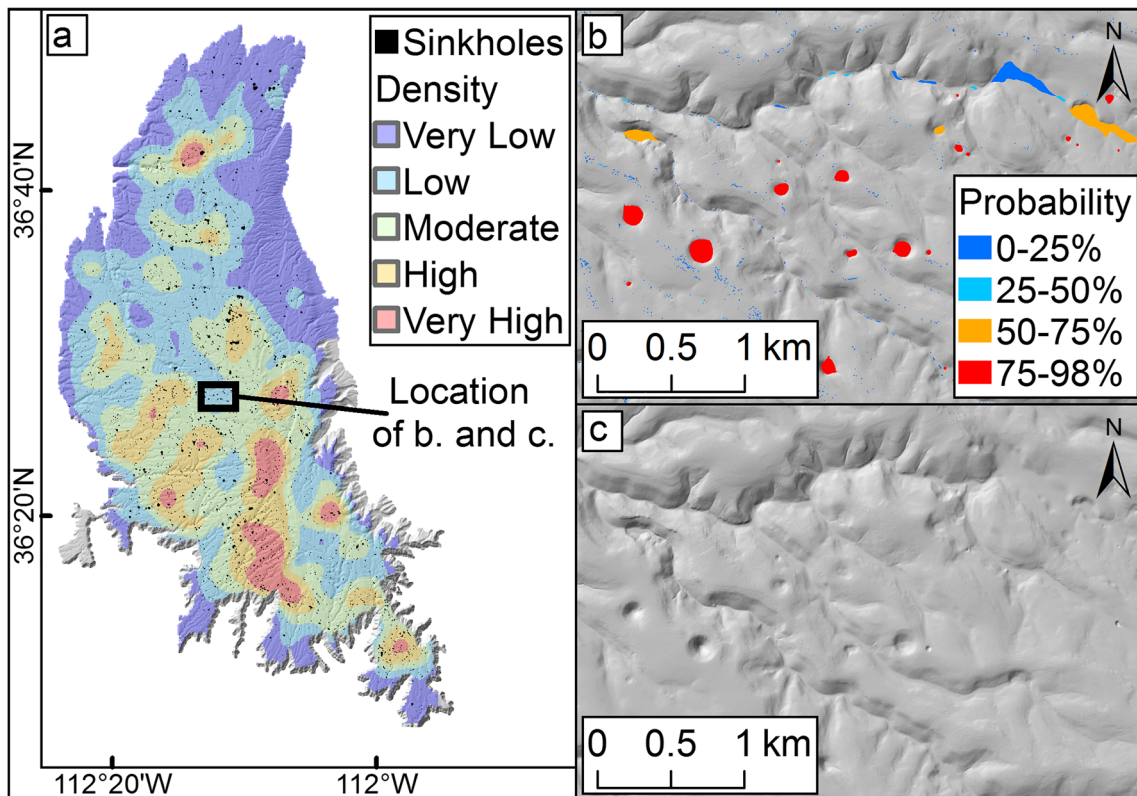


Fig. 4 a Shaded relief image of the Kaibab Plateau with the locations of 6,973 sinkholes overlaying a kernel density distribution of sinkhole density; b Close up of depressions and their sinkhole delineations, color coded according to the percent likelihood of being a sinkhole as estimated

by Random Forests, overlaying a shaded relief image created from the LiDAR DEM; c The same zoomed in view without the sinkhole delineations

Fig. 5 Two vulnerability models of the Kaibab Plateau perched Coconino aquifer created by the original COP method (a) and the modified COP method (b). Note that the modified model shows greater variation in vulnerability

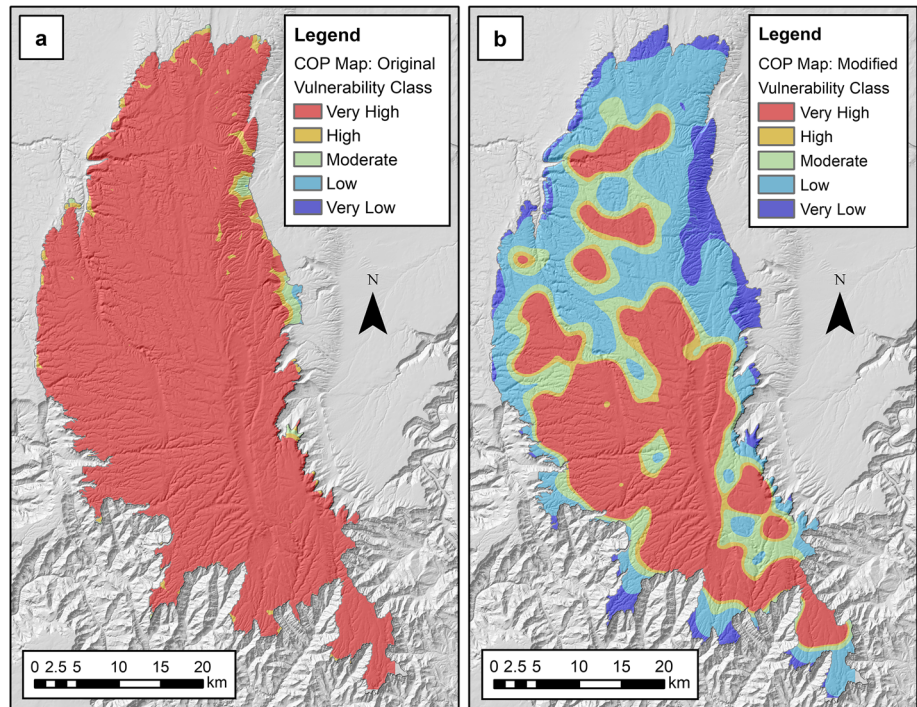
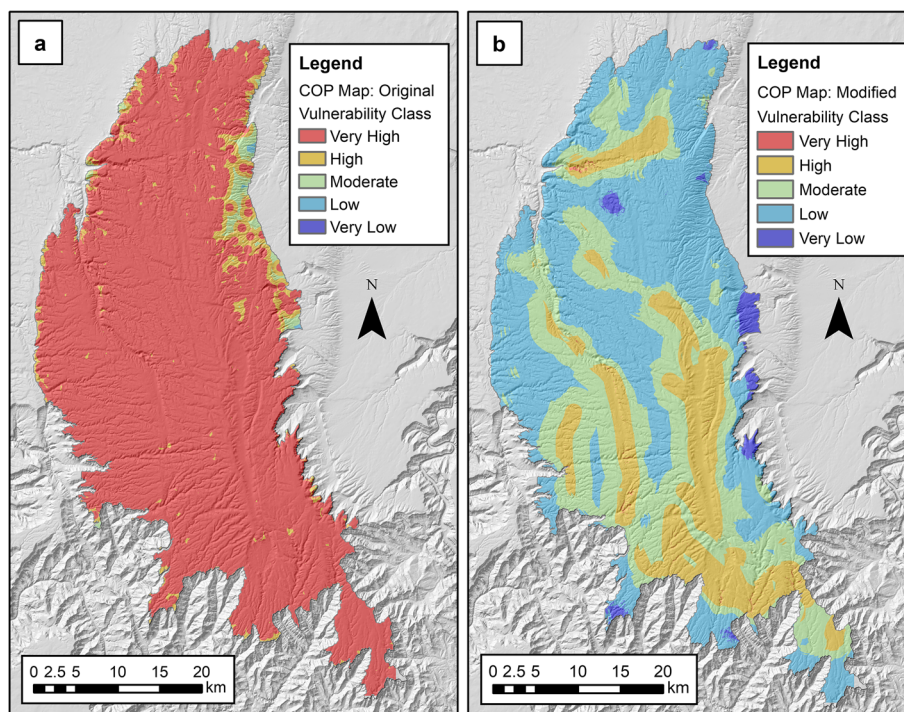


Fig. 6 Two vulnerability maps of the Kaibab Plateau deep R aquifer created by the original COP method (a) and the modified COP method (b). Note that the modified model has a reduced overall intrinsic vulnerability to contamination and greater spatial variation of vulnerability



represent the complexity of groundwater flow patterns that control infiltration, unsaturated zone flow, and contamination potential in arid and semi-arid regions, where semi-confining layers and substantial, thick unsaturated zones may reduce and diffuse flow concentration.

While R aquifer springs show rapid response times (Jones et al. 2017), they also show much longer residence times indicative of slower recharge and/or longer flow paths, which may reduce vulnerability (Tobin et al. 2018). It is likely that the overburden and the focusing of flow along faults reduces the vulnerability of the underlying R aquifer to contamination from waters transmitting into sinkholes distal from these fracture zones, and therefore it is unlikely that all sinkholes on the Kaibab plateau are connecting directly to this focused-recharge system. As such, not all sinkholes should be considered as highly vulnerable regions with respect to the R aquifer. The results of this study suggest that considering sinkhole

density and locations of faults is an appropriate approximate method of distinguishing this difference.

Conclusions

The modified COP models improved upon the original COP method by incorporating regionally significant recharge patterns to both shallow and deeper aquifers. The modified method used sinkhole density and faults to separately estimate vulnerability to contamination of the shallow, perched Coconino aquifer, and the deep, semiconfined R aquifer. The new method produced two vulnerability models containing greater variation of vulnerability and greater resolution of highly vulnerable regions of interest when compared to vulnerability models produced by the original COP method. Together, the two modified vulnerability models can facilitate better

Table 4 Percent distribution of vulnerability classes produced by each the four vulnerability models

Vulnerability class	Shallow aquifer (Coconino aquifer)		Deep aquifer (R aquifer)	
	Original COP	Modified COP	Original COP	Modified COP
Very high	97.2%	39.4%	94.0%	0.1%
High	2.0%	6.2%	4.6%	19.6%
Moderate	0.7%	14.6%	1.3%	30.3%
Low	0.1%	31.5%	0.1%	48.2%
Very low	0.0%	8.3%	0.0%	1.8%

Note that the original COP method estimates very high vulnerability for over 90% of the study area when applied to either the shallow or the deep aquifer

allocation of groundwater protection resources and inform scientists of which regions are primary spring recharge catchment areas. Correlations between sinkhole density and the presence of faults (Jones et al. 2017) strengthens the conceptual hydrologic models from which the methods in this paper are derived. Future research applying the method presented in this paper to other karst regions is encouraged, as this method can be applied to any karst aquifer regardless of stratigraphic complexity.

Acknowledgements Many thanks to all the peers and mentors that have helped with this project including Stefan Christie, Nick Steele, Mark Nebel, Krista Keski-Hynnala, Claire Spangenberg, Natalie Tanski, Coleman Hiatt, Alex Wood, Casey Jones, and many more.

Funding information Thank you to all sponsoring organizations that made this research possible including the Cooperative Ecosystem Studies Unit Grand Canyon Conservations, Conservation Legacy, AmeriCorps, GeoCorps, Geoscientist-in-the-parks program, northern Arizona University, Grand Canyon National Park, and Kaibab National Forest.

References

- Bear J (2007) *Hydraulics of groundwater*. Dover, Dover, Mineola, NY
- Billingsley GH, Hampton HM (2000) Geologic map of the Grand Canyon 30' × 60' quadrangle, Coconino and Mohave counties, northwestern Arizona. US Geol Surv Sci Invest Map: I-2688, scale 1:100,000. http://ngmdb.usgs.gov/geoDataGov/browse/34288_1.display.gif. Accessed October 2019
- Billingsley GH, Priest SS, Felger TJ (2008) Geologic map of the Fredonia 30' × 60' quadrangle, Mohave and Coconino counties, northern Arizona. US Geol Surv Sci Invest Map 3035, scale 1:100,000. <https://pubs.usgs.gov/sim/3035/>. Accessed October 2019
- Billingsley GJ, Stoffer PW, Priest SS (2012) Geologic map of the Tuba City 30' × 60' quadrangle, Coconino County, northern Arizona. <https://doi.org/10.3133/sim3227>. Accessed October 2019
- Breiman L (2001) *Random forests*, vol 45. <https://link.springer.com/content/pdf/10.1023/A:1010933404324.pdf>. Accessed October 2019
- Crossey LJ, Fischer TP, Patchett PJ, Karlstrom KE, Hilton DR, Newell DL, Huntoon P, Reynolds AC, de Leeuw GAM (2006) Dissected hydrologic system at the Grand Canyon: interaction between deeply derived fluids and plateau aquifer waters in modern springs and travertine. *Geology* 34(1):25. <https://doi.org/10.1130/G22057.1>
- Daly D, Dassargues A, Drew D, Dunne S, Goldscheider N, Neale S, Popescu I, Zwahlen F (2002) Main concepts of the “European approach” to karst-groundwater-vulnerability assessment and mapping. *Hydrogeol J* 10(2):340–345. <https://doi.org/10.1007/s10040-001-0185-1>
- Davis JC (2002) *Statistics and Data Analysis in Geology*, Third Edition. Wiley. isbn 0471172758
- Doerflinger N, Jeannin PY, Zwahlen F (1999) Water vulnerability assessment in karst environments: a new method of defining protection areas using a multi-attribute approach and GIS tools (EPIK method): cases and solutions environmental geology, vol 39. Springer. <https://doi.org/10.1007/s002540050446.pdf>
- ESRI (2016) ArcGIS desktop: release 10.5. Environmental Systems Research Institute, Redlands, CA
- Ford D, Williams P (2007) *Karst hydrogeology and geomorphology*. Wiley, West Sussex, UK. <https://doi.org/10.1002/9781118684986>
- Goldscheider N, Klute M, Sturm S, Hotzl H (2000) The PI method: a GIS-based approach to mapping groundwater vulnerability with special consideration of karst aquifers. *Zeitschrift Angewandte Geol* 46(3):157–166
- Goldscheider N, Drew D (2007) *Methods in karst hydrogeology*. International Contributions to Hydrogeology 26. International Association of Hydrogeologists.
- Guastaldi E, Graziano L, Liali G, Brogna FNA, Barbagli A (2014) Intrinsic vulnerability assessment of Saturnia thermal aquifer by means of three parametric methods: SINTACS, GODS and COP. *Environ Earth Sci* 72(8):2861–2878. <https://doi.org/10.1007/s12665-014-3191-z>
- Healy RW (2010) Estimating groundwater recharge-estimating groundwater recharge. www.cambridge.org. Accessed October 2019
- Hill CA, Polyak VJ (2010) Karst hydrology of Grand Canyon, Arizona, USA. *J Hydrol* 390(3–4):169–181. <https://doi.org/10.1016/j.jhydrol.2010.06.040>
- Huntoon PW (1970) *The Hydro-Mechanics of the Ground Water System in the Southern Portion of the Kaibab Plateau, Arizona*. University of Arizona, Ph.D., 1970, Copyrighted by P. W. Huntoon.
- Huntoon PW (1974) The karstic groundwater basins of the Kaibab plateau, Arizona. *Water Resour Res* 10(3):579–590. <https://doi.org/10.1029/WR010i003p00579>
- Huntoon PW (1981) Fault controlled ground-water circulation under the Colorado River, Marble Canyon, Arizona. *Ground Water* 19(1):20–27. <https://doi.org/10.1111/j.1745-6584.1981.tb03433.x>
- Huntoon PW (2000) Variability of karstic permeability between unconfined and confined aquifers, Grand Canyon region, Arizona. *Environ Eng Geosci* 6(2):155–170. <https://doi.org/10.2113/gsegeosci.6.2.155>
- Iván V, Mádl-Szonyi J (2017) State of the art of karst vulnerability assessment: overview, evaluation and outlook. *Environ Earth Sci* 76: 112. <https://doi.org/10.1007/s12665-017-6422-2>
- Jones CJ, Springer AE, Tobin BW, Zappitello SJ, Jones NA (2017) Characterization and hydraulic behaviour of the complex karst of the Kaibab plateau and Grand Canyon National Park, USA. *Geol Soc Spec Publ* 466(1). <https://doi.org/10.1144/SP466.5>
- Kass Green and Associates (2009) *Geospatial data for the Vegetation Mapping Inventory Project of Grand Canyon National Park/Parashant National Monument*. Integrated Resource Management Applications. National Park Service. http://irmaservices.nps.gov/arcgis/rest/services/Inventory_Vegetation/Vegetation_Map_Service_for_Grand_Canyon_National_Park_and_Parashant_National_Monument/MapServer. Accessed October 2019
- Kavouri K, Plagnes V, Tremoulet J, Dörflinger N, Rejiba F, Marchet P (2011) PaPRIKa: a method for estimating karst resource and source vulnerability-application to the Ouyssse karst system (Southwest France). *Hydrogeol J* 19(2):339–353. <https://doi.org/10.1007/s10040-010-0688-8>
- Li W, Goodchild MF, Church R (2013) An efficient measure of compactness for two-dimensional shapes and its application in regionalization problems. *International Journal of Geographical Information Science* 27(6):1227–1250
- Lindsey BD, Katz BG, Berndt MP, Ardis AF, Skach KA (2010) Relations between sinkhole density and anthropogenic contaminants in selected carbonate aquifers in the eastern United States. *Environ Earth Sci* 60(5):1073–1090. <https://doi.org/10.1007/s12665-009-0252-9>
- Ludington S, Moring BC, Miller RJ, Flynn KS, Hopkins MJ, Haxel GA (2005) Preliminary integrated databases for the United States: western states—California, Nevada, Arizona, and Washington. US Geol Surv Open File Report 2005-1305. <http://pubs.usgs.gov/of/2005/1305>. Accessed October 2019
- Marín AI, Dörflinger N, Andreo B (2012) Comparative application of two methods (COP and PaPRIKa) for groundwater vulnerability mapping in Mediterranean karst aquifers (France and Spain). *Environ*

- Earth Sci 65(8):2407–2421. <https://doi.org/10.1007/s12665-011-1056-2>
- McKee ED (1969) Paleozoic Rocks of Grand Canyon, Geology and Natural History of the Grand Canyon Region, Fifth Field Conference, Powell Centennial River Expedition, 1969 Pages 78–90 Retrieved from http://archives.datapages.com/data/fcgs/data/009/009001/78_four-corners090078.htm
- McKee ED, Gutschick RC (1969) History of the Redwall Limestone of northern Arizona. The Geological Society of America, Boulder, CO. <https://doi.org/10.1130/MEM114-p1>
- McKee ED, Resser CE (1945) Cambrian history of the Grand Canyon region: part I, stratigraphy and ecology of the Grand Canyon. Carnegie Institution of Washington, Washington, DC
- Miao X, Qiu X, Wu SS, Luo J, Gouzie DR, Xie H (2013) Developing efficient procedures for automated sinkhole extraction from Lidar DEMs. *Photogramm Eng Remote Sens* 79(6):545–554. Retrieved from www.news-leader.com
- Moreno-Gomez M, Pacheco J, Leidl R, Stefan C (2018) Evaluating the applicability of European karst vulnerability assessment methods to the Yucatan Kars, Mexico. *Environ Earth Sci* 77:682. <https://doi.org/10.1007/s12665-018-7869-5>
- National Oceanic and Atmospheric Administration (NOAA) (2013) Bright Angel Ranger Station COOPID 21001, data for the period 1948–2013. <https://www.ncdc.noaa.gov/cdoweb/datasets/GHCND/stations/GHCND:USC00021001/detail>. Accessed October 2019
- O'Donnell FC, Flatley WT, Springer AE, Fulé PZ (2018) Forest restoration as a strategy to mitigate climate impacts on wildfire, vegetation, and water in semiarid forests. *Ecol Appl* 28(6):1459–1472. <https://doi.org/10.1002/eap.1746>
- Panno SV, Angel JC, Nelson DO, Pius Weibel C, Luman DE (2008) Sinkhole distribution and density of Columbia Quadrangle Monroe and St. Clair counties, Illinois. <http://www.isgs.uiuc.edu>. Accessed October 2019
- Panno SV, Kelly WR, Angel JC, Luman DE (2013) Hydrogeologic and topographic controls on evolution of karst features in Illinois' sinkhole plain. *Carbon Evapor* 28:13–21. <https://doi.org/10.1007/s13146-013-0157-2>
- Polemio M, Casarano D, Limoni PP (2009) Karstic aquifer vulnerability assessment methods and results at a test site (Apulia, southern Italy). *Hazards Earth Syst Sci* 9. <https://doi.org/10.5194/nhess-9-1461-2009>
- Ravbar N, Goldscheider N (2007) Proposed methodology of vulnerability and contamination risk mapping for the protection of karst aquifers in Slovenia. *Acta Carsologica* 36(3):397–411. <https://doi.org/10.3986/ac.v36i3.174>
- Salford Systems (2016) Salford predictive modeler. Salford, San Diego, CA. <https://www.salford-systems.com/products/spm>. Accessed October 2019
- Scanlon BR, Healy RW, Cook PG (2002) Choosing appropriate techniques for quantifying groundwater recharge. *Hydrogeol J* 10:18–39. <https://doi.org/10.1007/s10040-0010176-2>
- Scanlon BR, Keese KE, Flint AL, Flint LE, Gaye CB, Edmunds WM, Simmers I (2006) Global synthesis of groundwater recharge in semi-arid and arid regions. *Process* 20:3335–3370. <https://doi.org/10.1002/hyp.6335>
- Tobin BW (2013) Contributions of karst groundwater to water quality and quantity in a mountain river basin: the Kaweah River, Sequoia and Kings Canyon national parks, California. PhD Thesis, Texas State University. <https://digital.library.txstate.edu/handle/10877/4698>. Accessed October 2019
- Tobin BW, Springer AE, Kreamer DK, Schenk E (2018) Review: The distribution, flow, and quality of Grand Canyon Springs, Arizona (USA). *Hydrogeol J* 26(3):721–732. <https://doi.org/10.1007/s10040-017-1688-8>
- USDA Forest Service, Region 3 (2009) Mid-scale existing vegetation dominance type map units of the Coconino and Kaibab NFs. USDA Forest Service, Albuquerque, NM. https://ds.fs.fed.us/EFS/FS/NFS/R03/Program/7140Geometrics/GISstaff/Workspace/jmoreland/Rcrawford/Website/Data/KAI/S_R03_KAI_dominance_type_map_units.shp. Accessed October 2019
- Vías JM, Andreo B, Perles MJ, Carrasco F, Vadillo I, Jiménez P (2006) Proposed method for groundwater vulnerability mapping in carbonate (karstic) aquifers: the COP method. *Hydrogeol J* 14(6):912–925. <https://doi.org/10.1007/s10040-006-0023-6>
- Watershed Sciences (2012) Kaibab National Forest LiDAR data report. Watershed, Corvallis, OR. www.wsidata.com. Accessed October 2019
- White WB (1988) *Geomorphology and hydrology of karst terrains*, 1st edn. Oxford University Press, Oxford, UK
- Wilson ED, Moore RT, Cooper JR (1983) Digital geologic map of Arizona: a digital database derived from the 1983 printing of the Wilson, Moore, and Cooper 1:500,000-scale map. US Geol Surv Open File Rep 00-409. <http://pubs.usgs.gov/of/2000/0409/>. Accessed October 2019
- Zevenbergen LW, Thorne CR (1987) Quantitative analysis of land surface topography. *Earth Surface Processes and Landforms* 12(1):47–56
- Zhu J, Pierskalla WP (2016) Applying a weighted Random Forests method to extract karst sinkholes from LiDAR data. *J Hydrol* 533:343–352. <https://doi.org/10.1016/j.jhydrol.2015.12.012>
- Zwahlen F (2004) Vulnerability and risk mapping for the protection of carbonate (karst) aquifers, final report (COST Action 620). European Commission, Directorate XII Science, Research and Development, Report EUR 20912, Brussels, p 297